Sensitivity of asymmetric rate-dependent critical systems to initial conditions: Insights into cellular decision making

Nuno R. Nené,[1,2,*] James Rivington,[3] and Alexey Zaikin[2,3,4]

[1]*Department of Genetics, University of Cambridge, CB2 3EH Cambridge, United Kingdom*
[2]*Institute for Women's Health, University College London, Gower Street, WC1E 6BT London, United Kingdom*
[3]*Department of Mathematics, University College London, Gower Street, WC1E 6BT London, United Kingdom*
[4]*Department of Applied Mathematics, Lobachevsky State University of Nizhny Novgorod, Nizhny Novgorod, Russia*

(Received 6 February 2018; revised manuscript received 29 June 2018; published 22 August 2018)

The work reported here aims to address the effects of time-dependent parameters and stochasticity on decision making in biological systems. We achieve this by extending previous studies that resorted to simple bifurcation normal forms, although in the present case we focus primarily on the issue of the system's sensitivity to initial conditions in the presence of two different noise distributions, Gaussian and Lévy. In addition, we also assess the impact of two-way sweeping at different rates through the critical region of a canonical Pitchfork bifurcation with a constant external asymmetry. The parallel with decision making in biocircuits is performed on this simple system since it is equivalent in its available states and dynamics to more complex genetic circuits published previously. Overall we verify that rate-dependent effects, previously reported as being important features of bifurcating systems, are specific to particular initial conditions. Processing of each starting state, which for the normal form underlying this study is akin to a classification task, is affected by the balance between sweeping speed through critical regions and the type of fluctuations added. For the heavy-tailed noise, two-way dynamic bifurcations are more efficient in processing the external signals, here understood to be jointly represented by the critical parameter profile and the external asymmetry amplitude, when compared to the system relying on escape dynamics. This is particular to the case when the system starts at an attractor not favored by the asymmetry and, in conjunction, when the sweeping amplitude is large.

DOI: 10.1103/PhysRevE.98.022317

I. INTRODUCTION

The fidelity with which cellular systems respond to external signals has generated an increasing interest in quantifying the resultant downstream effects that elicit dynamic responses [1–4]. The idea of robustness in the face of external drivers has also been prevalent in other areas, particularly in evolutionary biology. There, systems are seen, to an extent, as being the result of continuously changing environments determining fitness [5,6]. In more clinically oriented applications, albeit in the realm of evolutionary biology, the idea of an external control has also been important in the design of adaptive and optimal therapies [7,8]. Adding to this body of work, recent developments in biopattern formation have shown that path-dependent effects imposed by external sources are a significant component of observed phenotypic outcomes [9]. The subject of an external driver inducing bifurcations in the underlying intrinsic dynamics, as is the case of the system studied here, has been less debated in biology. The study of such systems opens up several research avenues that have only recently attracted considerable interest [10–12]. Therefore, there is scope for extensive testing, from a computational point of view, of relevant features prevalent in the literature of open systems [13–17].

In this work, we extend previous studies that sought applications in network biology [11,12,18,19]. Specifically, we address the question of cellular decision making through the lenses of simpler canonical problems and the idea of dynamic bifurcations; below we provide the biological context and establish the equivalence between intricate genetic circuits and simpler normal forms. The main ingredients from the area of open systems undergoing critical transitions that we will resort to here are the following: critical parameter time dependence, passage through a critical region at different rates, and stochasticity hindering the convergence to any of the emerging states.

A representative low-order circuit underlying studies of cellular decision making, the integrative signaling-gene regulatory switch, is depicted in Fig. 1(a); its structure can be tweaked so as to resemble other circuits behind observed phenomena (see, for example, Ref. [20]). In this context, cellular decision making is understood as the circuit responding consistently and accurately to the combination of external signals, by turning on specific activity patterns of the downstream nodes [see Fig. 1(a)]. In the same figure, we also show the phase diagram corresponding to a set of nonlinear differential equations, including activation, translation, and transcription of crucial proteins, in this case transcription factors. By varying the values of signals S_1 and S_2, which in the case of Fig. 1(a) work as the external drivers, we are able to generate typical regimes observed in systems relevant to experiments [10,21,22]. The mechanism of Speed-dependent Cellular Decision Making (SdCDM) [11], which arises from crossing the critical region ($I_{L,H}$ to II_A) at different rates, is one of such regimes. Here,

*Corresponding author: nunonene@gmail.com

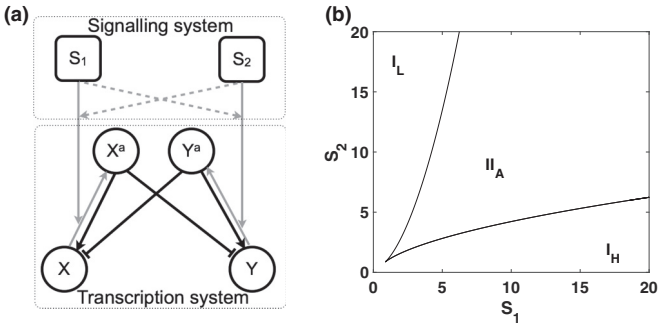

FIG. 1. Representative low-order genetic switch with external stimulation. (a) Schematic representation of circuit: nodes X and Y stand for transcription factors that can be activated to generate X^a and Y^a, respectively. $S_{1,2}$ represents external or upstream signals inducing the activation of downstream nodes; black lines represent transcriptional reactions, leading to induction or repression of production of X and Y; gray lines depict activation or protein-protein interactions. (b) Phase diagram in the space of (S_1, S_2). Thin lines represent borders between different regimes elicited by the external signals: $I_{L,H}$ stands for monostability, with X having a low (L) or a high value (H). II_A denotes bistability between two states at which X and Y have opposite concentrations, (H, L) or (L, H). See Ref. [11] for details of the underlying equations.

instead of relying on the integrative genetic switch once again, we will opt for simple standard norm forms that exhibit similar behaviors and regimes to those represented in Fig. 1(b). In fact, the effects of S_1 and S_2 can be economically modeled by a supercritical Pitchfork bifurcation normal form with coupled time-dependent critical parameter and external asymmetry [18]. This normal form has been successfully used in the study of genetic circuits behind, for example, decision making in hematopoietic cell differentiation regulated by $GATA1$ and $PU.1$ [10,21]. More recent work has also resorted to the idea of the bistable potential with external drivers in order understand the influence of signaling on expression dynamics in the $GATA$-$NANOG$ circuit in embryonic stem cells [22]. Despite the issue of bifurcations, or critical transitions, not making part of the model underlying the study reported in Ref. [22], their system can also be tested under the framework highlighted below and explored in Refs. [11,18].

Our choice of a standard normal form allows us to link our findings to previous theoretical work on dynamic bifurcations and, ultimately, serves as a bridge to investigations of the importance of rate-dependent effects in complex noisy genetic networks. The work presented here is, above all, an investigation into the sensitivity to initial conditions when all of the ingredients reported above are present. Unlike previously [18], we study the effects of both forward and reverse bifurcations when trajectories start in the bistability region. We further delve into the importance of fluctuations following different distributions: the typical Gaussian and that arising in the literature of Lévy processes in biology [23]. The latter is an important alternative when modeling transitions between states even when noise amplitudes are small; it constitutes a viable candidate for modeling cell fate decision as an escape problem [23–25]. Furthermore, the presence of a skewness parameter provides us with the option of modeling possible biases through an asymmetric noise distribution, which the Gaussian white noise cannot accommodate. The possibility of asymmetric noise distributions may be a relevant feature of biological systems under stress, where an association between a stimuli and an evolved response is not driven or strictly induced *per se*. The actual cellular decision-making outcome arises in the strength of numbers and average responses [26]. The use of this additional noise distribution can also contribute to the problem of noise-induced symmetry breaking in cellular circuits [27].

II. DYNAMICALLY BIFURCATING SYSTEMS WITH NOISE AND ASYMMETRIES

A. Forward bifurcations

A typical bifurcation representing decision making in biology [10,11] or second-order phase transitions in physical systems [13,28–32] is that underlying Eq. (1). In the case where the external asymmetry g is zero and the bifurcation parameter λ is independent of time, Eq. (1), which represents a supercritical Pitchfork normal form, has the unique asymptotically stable solution $x = 0$ when $\lambda < 0$. For positive values of λ, three solutions can be clearly shown to appear: the asymptotically stable branches given by $\pm\sqrt{\lambda}$ and the trivial unstable solution $x = 0$:

$$\dot{x} = \lambda(t)x - x^3 + g, \tag{1}$$

$$\lambda(t) = \lambda_0 + \gamma t. \tag{2}$$

In the work presented here, we are interested in the solutions of Eq. (1) when g is not zero. This asymmetry can be seen as a representation of discrepancies between upstream signals to a circuit regulating cell fate decision [see, for example, Fig. 1(a)] [18].

Making the asymmetry different from zero destroys the previous bifurcation point at $\lambda = 0$; a new picture emerges made of three branches at $\lambda = \lambda_c$: a connected set of solutions with positive values, x_+, a disconnected branch with negative values, x_-, and an unstable branch x_u [see Fig. 2(a)]. In this imperfect bifurcation the branches are separated by a minimum distance $d_{\min} = (\Delta X)_{\lambda=\lambda_c} = (x_+ - x_-)_{\lambda=\lambda_c} = 3(\frac{g}{2})^{\frac{1}{3}}$; as g is increased so is the distance between solutions at λ_c. In addition, the critical point λ_c is displaced towards positive values of λ by $3(\frac{g}{2})^{\frac{2}{3}}$ [18]. We should add that the connected and disconnected branches invert their positions if, contrary to Fig. 2(a), we impose a negative asymmetry. Other types of bifurcation have been selected as models of cell decision making in biology [10,20,21,33,34]. The idea behind the work presented here is still valid in those cases, although the framework has to be adapted for optimal representation.

As was explored in the previous work [18], our aim is to understand the effects of drivers on the behavior of a system regulated by Eq. (1). In Ref. [18] we studied the effect of a ramped bifurcation parameter [Eq. (2)] and a coupled time-dependent transient asymmetry $g(t)$. This work was motivated by integrative signaling-gene regulatory circuits (see Fig. 1) that exhibit the same critical behavior [11]. By studying the effect of sweeping the system through the critical region under different γ rates [Eq. (2)], in the presence of fluctuations, we

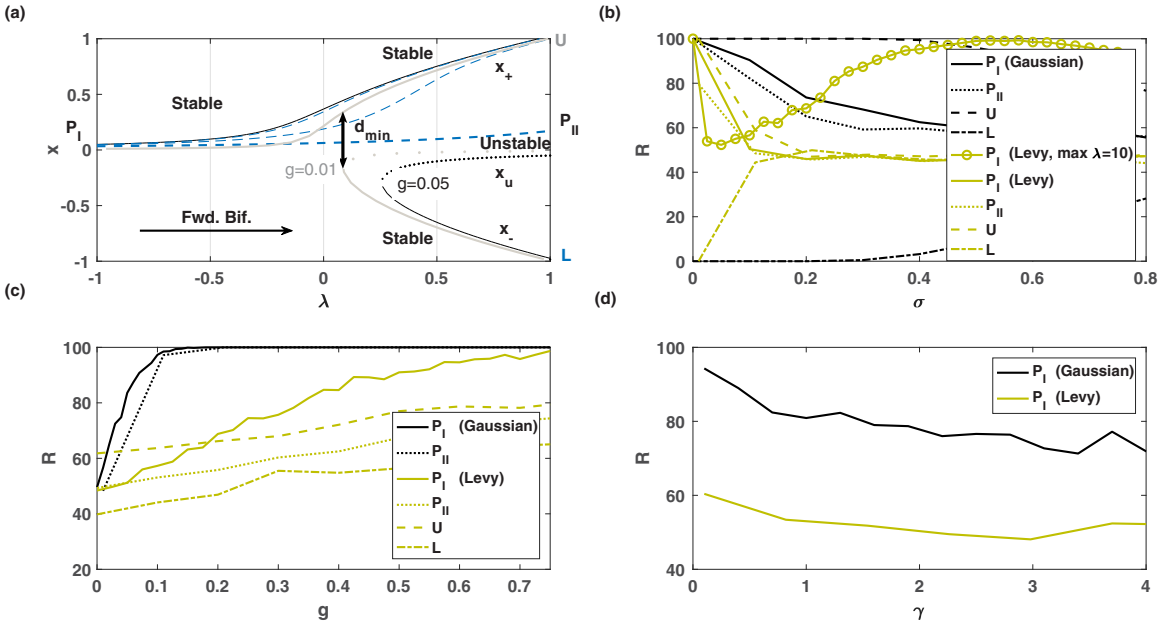

FIG. 2. Rate-dependent effects in forward dynamic bifurcations in conjunction with asymmetries and noise. (a) Bifurcation diagrams for $g = 0.01$ and $g = 0.05$. Also shown in blue are the deterministic trajectories for $g = 0.05$ when $\gamma = 0.01$ (thinner), 0.1 (intermediate), and 1 (thicker) [see Eqs. (1) and (2)]. The bifurcation diagram corresponds to the steady-state solutions of Eq. (1) for each value of λ. The deterministic trajectories correspond to numerical solutions of Eq. (1) when λ is time-dependent. The starting point for each trajectory is the stable state $x(\lambda = -1)$. The final value of λ during the one-way forward sweeping is 1. (b) Selectivity R with noise amplitude σ, for $g = 0.05$ and $\gamma = 1$, when the system starts at stable state $x(\lambda = -1)$, represented as P_I. The final value of λ during the sweeping process is 1. One case is plotted for comparison purposes where the maximum λ is 10. Also shown is the selectivity for the system when λ is held at 1, and, additionally, the initial conditions are at the upper branch (U), lower branch (L), and the point equal to the steady state $x(\lambda = -1)$ (P_{II}). In these three additional cases the final value of R is dependent only on branch-to-branch transitions. (c) Selectivity R with asymmetry g, for $\sigma = 0.1$ and $\gamma = 1$. For the P_I lines the initial and final values of λ during the sweeping process are -1 and 1, respectively. As in (b) we also show results for the case where λ is not swept and remains equal to 1. Curves for starting points U and L did not change with g and are not shown. (d) Selectivity R with sweeping speed γ, when $g = 0.05$ and $\sigma = 0.1$. All other parameters are as above. Black lines: Gaussian noise. Green: Lévy noise, with $\mu = 1.8$, $c = 1/100$ and $\xi^u = 5$ [see Eqs. (6) and (5)]. One thousand trajectories were used in the calculation of R, the percentage attracted to x_+.

were able to prove the existence of speed-dependent effects in branch selectivity. The same holds for constant external asymmetries, even if they are much smaller than 1 [28,29]. In both cases, the percentage of trajectories (R, selectivity) in a stochastic simulation that are attracted to the branch favored by the asymmetry is proportional to Eq. (3), where σ represents the amplitude of fluctuations, g the asymmetry, γ the critical parameter sweeping speed [Eq. (2)], erf(·) the error function, and $\alpha = 0$ and $\beta = 1$ if g is constant. The expression for the selectivity R was obtained in previous work [18,28,29] by studying the first two moments of the distribution of trajectories when crossing the critical point λ_c. If the distribution is assumed to be Gaussian-like around the critical point, the first two moments can be used to calculate the area under the distribution that is above the unstable branch (for positive g). This is assumed to approximate the percentage of trajectories that reach the favored branch of solutions and leads, after some manipulation of the Fokker-Planck equation associated with Eq. (4), to R:

$$R \propto \frac{1}{2}\left(1 + \mathrm{erf}\left\{\frac{g}{\sigma}\left[\alpha + \beta\left(\frac{\pi}{\gamma}\right)^{\frac{1}{4}}\right]\right\}\right) \times 100. \qquad (3)$$

Two of the main contributors to the sensitivity of the system to the effect of the external asymmetry, in addition to noise amplitude (σ) and sweeping rate (γ), is the inflexion of the connected branch and the position of λ_c [observe Fig. 2(a)] [18,28,29,35]. These factors, in conjunction with lower sweeping speeds, increase branch selectivity in a significant way due to lower switching delays [14,18,28,29,35]; these are defined as the additional time spent near the potential unstable boundary after the system goes through the critical point [14]. This result is observed even if the amplitude of fluctuations with respect to the asymmetry is large [18]. In fact, the switching delay dependence on sweeping speed can be clearly verified in Fig. 2(a), where several deterministic trajectories are plotted for a constant $g = 0.05$. The system was initially started at the stable branch for $\lambda = -1$ and λ was subsequently changed according to the linear law represented in Eq. (2). As is evident, lower sweeping rates induce paths that are further away from the unstable state when the critical region emerges. The instant where the switch begins can be demonstrated to be proportional to $1/\gamma$, a factor that also influences the probability of reaching the branch favored by g when fluctuations are incorporated [18,28,30,36,37]. The effects of g also reduce the probability of escape over the potential barrier, located along the unstable

state, which can be estimated to be located at $-\frac{g}{\lambda-\lambda_c}$ far beyond λ_c. The timescales and probability for these transitions can be modeled under the Kramer's classical theory [38].

1. The effect of noise model on branch selectivity in forward only bifurcations

One of the motivations for the work presented here is understanding if differences in noise distribution affect differently the system's memory of initial positions. In addition, we also aim to verify once again if rate-dependent effects are still a determinant in final state selection. Our previous work tested the system's memory of transient signals when it was driven through the critical region in one direction only [11,18]. Here we change slightly the scope and invest in simulations that highlight both the effect of initial conditions and a two-way sweeping or forward-reverse bifurcation scenario. This is closer to the situations observed in experimental biology where signals often have a transient character [39] or more complex profiles [4,40].

Before evaluating the forward-reverse dynamic bifurcation scenario, let us first address the simple system represented in Fig. 2(a) when fluctuations are present [$\xi(t)$ in Eq. (4)], so that we pin down the crucial aspects underlying branch selectivity for the noise distributions tested here:

$$\dot{x} = \lambda(t)x - x^3 + g + \sigma\xi(t). \tag{4}$$

As expected from the diagram represented in Fig. 2(a) and the deterministic trajectories plotted in blue, the overall shape of the distribution of trajectories when the control parameter λ is passed through the critical region is approximately Gaussian; at the same time it gradually drifts due to the positive external asymmetry g. Along with this bias in the process, the distribution also spreads up to the point where the critical value is reached $\lambda = \lambda_c = 3(\frac{g}{2})^{\frac{2}{3}}$; at this moment it starts reflecting the bimodality exerted by the bistability region [18]. Around the critical region and just before the onset of bistability, fluctuations are amplified and the convergence times towards the attractor are hindered. This may be counterbalanced, on the other hand, by a strong eternal field in conjunction with a slowly changed λ [Figs. 2(c) and 2(d)] [18,28,37].

Two distributions were tested for the noise term $\xi(t)$ in Eq. (4): the standard Gaussian and the Lévy distribution. The assumption of a Gaussian is consistent with previous work [18,28,29,32] and follows the typical assumptions in the literature: zero mean and correlation $\langle\xi(t), \xi(t')\rangle = dt\delta(t-t')$. The Lévy noise term is, on the other hand, less common. Its usage in biology was recently proven to be a valid approach to studying the effect of fluctuations in bistable systems [23]. We resort to this additional noise paradigm with the intent of understanding if the long tail characteristic of the Lévy distributed noise influences considerably the memory of initial conditions. This follows from the work on the role of stochasticity in biology as a major determinant of cell decision outcomes in different environments, by way of crossing or escaping over potential barriers [23–25] or by noise-induced symmetry breaking [27].

In order to test the Lévy noise it was necessary to truncate the distribution at an upper level, thus avoiding impractical extreme values. The percentile function for a Lévy distribution truncated to the support $\xi \in [\mu, \xi^u]$, where μ is the normal lower truncation due to the shift parameter μ and ξ^u is the upper truncation level, can be observed in Eq. (5), where $F(\xi)$ is the Lévy cumulative density function [Eq. (6)]:

$$p(\xi) = \frac{c}{2[\mathrm{erfc}^{-1}(F(\xi^u)\xi)]^2} + \mu, \tag{5}$$

$$F(\xi) = \mathrm{erfc}\left(\sqrt{\frac{c}{2(\xi-\mu)}}\right). \tag{6}$$

Here c is the scale parameter of the Lévy distribution and $\mathrm{erfc}^{-1}(x)$ the inverse complementary error function.

The R profile of the system perturbed by Lévy noise is equivalent to that observed with Gaussian noise when we start at point P_I, i.e., before the bifurcation ensues, although it is shifted. As expected, given that the Lévy distribution imposes higher fluctuations at the same amplitude, it generates selectivities that are lower than the standard Gaussian. The clear bias arising from the heavy tail in the Lévy distribution is, therefore, not observed for the λ sweeping amplitude from -1 to 1. If, on the other hand, we increase the maximum sweeping amplitude to $\lambda = 10$, a contrasting profile of R versus σ is recorded [see Fig. 2(b)]. When varying the noise intensity parameter in this scenario for the Lévy distributed noise model (with $g = 0.05$, $\gamma = 1$), we observe that for $\sigma \leqslant 0.08$ it follows a similar behavior to the Gaussian distributed model, where the percentage of paths attracted to each attractor decreases as the fluctuations amplitude increases [Fig. 2(b)]. Yet, contrary to the Gaussian model, for $\sigma > 0.08$, the probability of reaching the attractor favored by the asymmetry then converges towards 1. To gain an understanding of the general path behavior leading to the results discussed here, we have to recall that when crossing the σ threshold observed in Fig. 2(b), a qualitatively different regime ensues. Beyond λ_c, branch-to-branch transitions can occur that hinder the identification of the signal represented by g. Since the propensity for transitions to take place is larger with Lévy noise, the percentage of trajectories reaching x_+ should further decrease in a much more significant way. Nevertheless, there are two fundamental components at play. First, the escape rate diminishes as λ reaches higher values, especially from x_+ to x_-; this arises from the difference between the potential associated with $x_{+,-}$ and x_u becoming larger as λ is swept [32]. Therefore, the potential difference traps the system in x_+ due to g. On another side, if the simulations are long enough, the chances of converging towards the positive branch are higher due to the positive heavy-tailed Lévy noise term. Consequently, for sufficiently large noise amplitudes and longer trajectories, a greater percentage of paths eventually converge to the positive attractor basin as the synergy between the two components emphasized above is stronger than the destructive power of fluctuations. This explains the unusual curve in Fig. 2(b), when the initial condition is at P_I and λ is driven through the critical region and ends at much higher values.

The effect of the asymmetry g as a state selector can be visualized in Fig. 2(c). For both noise distributions the capture of the trajectories by the upper branch, for a constant sweeping rate $\gamma = 1$, is more efficient for higher values of g. As mentioned above, this results, once more, from both the position of the critical value λ_c and the inflexion of the upper branch [see also Eq. (3) for an approximate expression]. This observation had been made in previous publications [11,18] and follows

intuitively from the observation of the deterministic trajectories depicted in Fig. 2. For these specific results, the noise amplitude used is around the threshold mentioned in a previous paragraph, $\sigma \approx 0.08$, and the sweeping of parameter λ is done from -1 to 1. The evaluation of the impact of the external asymmetry as a state selector is, therefore, not confounded with the effects of the positive heavy tail of the Lévy distribution [Fig. 2(b)].

Cell decision making has been widely modeled as a process where the most probable outcome is already encoded in the distribution of attractors; this perspective sees the desired decision outcomes arising simply by attractor to attractor transitions induced by noise (see, for example, Ref. [23]). Here, as was the case of previous publications by some of the authors of this study, we evaluate a different decision-making paradigm. Nevertheless, it is important to verify which scenario is more efficient in processing information. In Figs. 2(b) and 2(c), the values of R computed when λ is time-dependent and follows Eq. (2) can be compared with those when it is held at its maximum. In the latter, branch selectivity is solely determined by escape dynamics, not the dynamic bifurcation. Overall, when λ is held at 1, the Gaussian term requires much larger noise amplitudes to tilt the percentage towards lower values and is, therefore, ineffective in eliciting jumps over the potential barrier. The Lévy distributed noise allows, on the other hand, for jumps to occur across the potential barrier, which explains the tendency for R to reach lower values at much lower noise amplitudes. Measuring the selectivity obtained under a dynamic bifurcation [starting point P_I in Figs. 2(b) and 2(c)], with a comparable situation resulting from escape over the potential barrier [starting point P_{II} in Figs. 2(b) and 2(c)], we verify that, over most σ's and asymmetries, crossing through the critical region enhances selectivity. This is a fundamental result for understanding the results in the forward-reverse dynamic bifurcation explored in Sec. II B; it arises from the disconnection between branches and the inflection near the critical region [see discussion at the beginning of the section and Fig. 2(a)].

Regarding the rate-dependent effects on the propensity for reaching the attractors favored by g, it is clear that this state selection mechanism is present when both noise distributions are used [Fig. 2(b)]. As observed in previous studies [18], larger γ's destroy the bias exerted by g, a consequence felt stronger if the heavy-tailed noise distribution is imposed.

B. Forward-reverse bifurcations

Typical external signals in biology have complex profiles [40], and adequate responses to each of the signal characteristics have to occur, to an extent, in the induced expression patterns [39,41]. Previously, we proved that the switching delays and the asymmetries in expression patterns induced by external signals can be understood by the simple normal forms represented in Eq. (1) [11,18] (see also Sec. II A). Yet, as remarked before, the effect of signals on decision making does not push the system in one direction only as they usually return to basal levels; this clearly induces crossing of the critical region in the reverse direction [39] [see Fig. 3(a)]. Moreover, the nature of signals and networks in biology dictates that the drivers are often compounded [32] and stochastic [4]. A forward-reverse simulation experiment stands, therefore, as a closer representation of the dynamical behavior of the typical circuitry determining cellular decision making. An interesting contribution to the subject of recurrent bifurcations was also explored through deterministic forcings, although the effects of stochasticity were not approached [42] and the motivation was not the study of biological networks. Here, in order to understand the main ingredients at play in these complex scenarios, we generalize the sweeping process in both directions; the system starts in the bistability region, crosses into the monostability region, and inverts the movement back to the parameter value it started. This is represented in Fig. 3(a), which can be reproduced by changing $\lambda(t)$ to $-\lambda(t)$ in Eq. (1).

1. Effects of sweeping speed and stochasticity for different initial conditions

The scenario explored in Sec. II A helps us to understand each stage of the experiment represented in Fig. 3(a): the forward sweeping segment destroys the memory of the initial conditions; the backward segment, studied in Sec. II A, takes the degradation of the initial information encoded in the state of the system at the point of reversal, and either recovers the position at $t = 0$ or, due to action of fluctuations and the convergence properties of the system, completely forgets its initial state. It should be pointed out that, for a particular sweeping speed γ, if the sweeping amplitude is large enough, convergence to the upper branch is always present in a deterministic setting [see trajectories in Fig. 3(a)]; under these circumstances, if the system starts at the lower part of the diagram, memory of any initial conditions in this region is destroyed. Yet, as we are, in fact, modeling the presence of fluctuations [$\xi(t)$ in Eq. (4)], which represent stochastic processes inherent to each stage of the integrative genetic circuits [1–4,43], there is always a hindrance to the capacity of the system to respond to external signals, represented here by the joint action of the time-dependent profile of λ and g. In this sense, both sources contain features that are processed by the normal form in the presence of noise. The initial condition $x(0)$ constitutes the third source.

If we start the system at U, L, or I represented in Fig. 3(a), it either retains or loses the memory of the initial instant while responding and processing $\lambda(t)$ and g. During the forward segment the trajectories tend to converge to the only available steady-state solution after crossing the critical region at $-\lambda_c$. This convergence is affected by the same parameters as the scenario explored in a previous section where one-way only sweeps were included. If the sweeping speed is sufficiently low, the system definitely converges. Once λ is forced back to the starting point, during the backward segment, the propensity to be captured by the basin of attraction of the branch favored by g changes much more if the simulations start at L and I. In either, larger sweeping rates reduce the sensitivity of the system to g but increase the likelihood of maintaining memory of the initial condition [see Fig. 3(c)]; lower sweeping rates have the opposite effect. The reasons behind this can also be understood by inspecting the deterministic trajectories in Fig. 3(a). Since given enough sweeping amplitude convergence to the upper branch is always observed in a deterministic

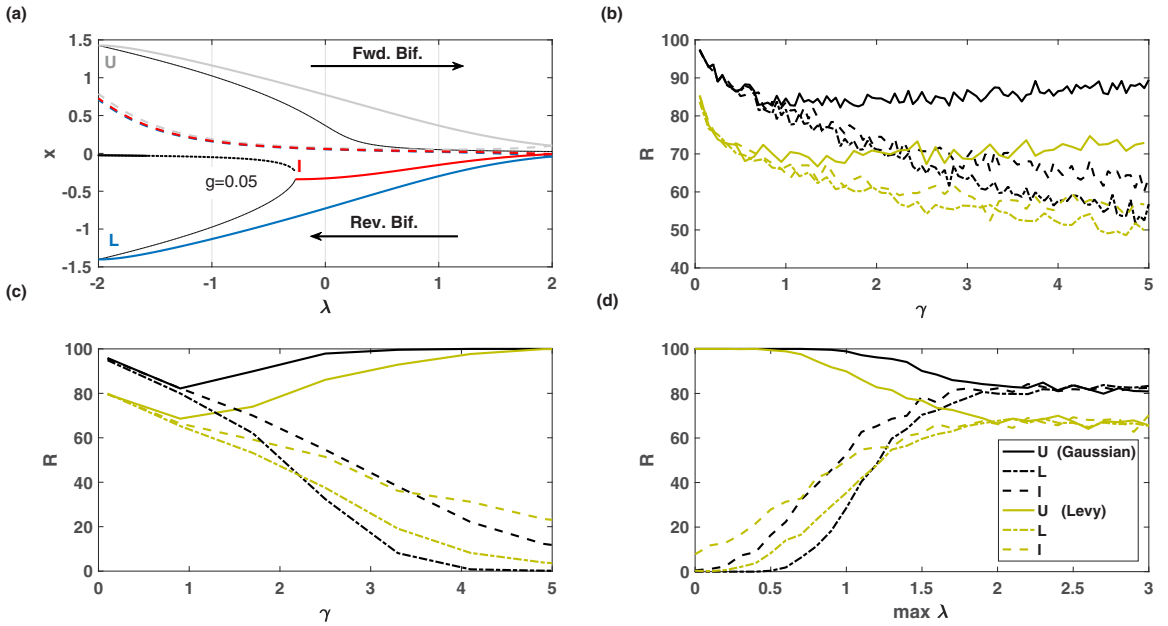

FIG. 3. Sensitivity of branch selectivity to initial conditions, sweeping speed, and amplitude in forward-reverse dynamic bifurcations. (a) Bifurcation diagram (black) indicating sweeping directions, starting conditions, and deterministic trajectories. U: starting position at the steady state at upper branch for $\lambda_0 = -2$ (gray). I: starting position at the intermediate steady state for $\lambda_0 = \lambda_c = 3(\frac{g}{2})^{\frac{2}{3}}$ (red). L: starting position at the lower steady state for $\lambda_0 = -2$ (blue). Thick full lines and dashed lines represent forward and backward sweeping, respectively. The bifurcation diagram corresponds to steady-state solutions of Eq. (1) for each value of λ. The deterministic trajectories correspond to numerical solutions of Eq. (1) when λ is time-dependent. (b) Selectivity R with $\gamma_{\text{Fwd}} = 1$ and $\gamma_{\text{Rev}} = \gamma$. (c) Selectivity R with $\gamma_{\text{Fwd}} = \gamma_{\text{Rev}} = \gamma$. (d) Selectivity R with $\gamma_{\text{Fwd}} = \gamma_{\text{Rev}} = 1$ and maximum amplitude of λ during the forward segment. Black lines: Gaussian noise. Green: Lévy noise, with $\mu = 1.8$, $c = 1/100$ and $\xi^u = 5$ [see Eqs. (6) and (5)]. 1000 trajectories were used in the calculation of R, the percentage attracted to x_+. $g = 0.05$; $\sigma = 0.1$. Fwd: forward segment. Rev: reverse segment. For panels (a), (b), and (c) the maximum value of λ during the forward segment is 2.

setting, the likelihood of the system converging to the original lower branch is increased only if the differences in the system's relaxation timescale and that of $\lambda(t)$ are significantly different [14,29]. A similar reasoning holds for trajectories starting at U, although the convergence properties after reaching the monostable region are different. In this case, lower sweeping rates secure that the upper bifurcation branch x_+ is tracked at all times during the forward segment of the forward-backward experiment. If the same sweeping rate is held in the backward segment, the trajectories always track the connected branch and sensitivity to g is secured. In addition, memory of the initial condition is also present. Yet an interesting feature is verified when γ is increased from low values to values above 1. In this region, initially the trend is as expected: higher rates destroy information despite still helping to track the upper branch in the forward sweeping segment. Although the reverse segment is done at the same speed, at this stage it is sufficient to put the mean value among replicated trajectories closer to the unstable boundary which, as was explained above, enhances the propensity to jump across the potential barrier. On the other hand, the chances of remaining in the attractor basin of the upper branch, presuming we start at U, increase once again to very high values as we cross the threshold of $\gamma \approx 1$. This stems from not tracking the connected branch and the resulting distance to the stable solution once the monostability region is reached. Not being able to converge fast enough secures reduced branch to branch transitions once the system is reversed and, naturally, an improvement in R. This trend also occurs when Lévy noise is used, although consistently with its typical shape, selectivity is smaller than that achieved with the typical Gaussian noise. For the results pertaining to the starting points L and I, once again an interesting feature is observed when the heavy-tailed distribution is used. Despite an increase in sweeping rate inducing the expected results, the relative magnitude with respect to the results obtained with the Gaussian noise term is inverted at high enough γ's. This can also be attributed to the likelihood of larger positive deviations being more prevalent in the Lévy distribution, which, in combination with the fact that very large sweeping rates trap the system in the starting basin of attraction, improves the "apparent" relative sensitivity to g [see Fig. 3(c)].

Also regarding the importance of critical parameter sweeping speed in the forward and backward segments, Fig. 3(b) demonstrates that if γ_{Fwd} is held at 1 and γ_{Rev} is varied, the effects registered before for equal rates is less pronounced, despite the general tendency being the same. Therefore, differences in the sweeping segments may also be a potential mechanism for optimal cellular decision making. This is reminiscent of path-dependent effects recently observed in biocircuits regulating pattern selection [9], of expression dynamics behind stress-induced response [44], and, to an extent, of high-dimensional versions of the integrated circuit represented in Fig. 1(a) [12]. The combination of time-dependent signals and their shape [39], including ascending and descending rates, may have an influence on the probability of reaching certain attractors or cell fates.

2. Varying the elapsed time before system reversal

When simulating the system according to the same numerical recipe as that presented in the previous section, it is of interest to inspect how the amount of time elapsed before the system is reversed affects the number of paths attracted to each attractor. For maximum values of λ below 1, 100% of the paths converge to the positive steady state if the starting point is U and the noise model is Gaussian [see Figs. 3(a) and 3(d)]. This slowly decreases as maximum amplitudes of λ are gradually increased to 3. Attaining larger values of λ before reversal allows for the convergence of the system to the solutions represented by the upper branch, which is favored by the constant external asymmetry. This is fundamental because although the drift rate is approximately g, the relaxation to the equilibrium in the monostability region is quite slow for values of λ not far from λ_c; for example, at $\lambda = 0$, the position of the steady state is approximately $[g(\lambda = 0)]^{1/3}$, which makes the relaxation time $[g(\lambda = 0)]^{-2/3}$ [29]. Therefore, larger maximum amplitudes increase the convergence rate. On the other hand, proximity to the stable positive branch at large λ values implies proximity to the unstable branch if the sweeping speed is sufficiently high once the critical parameter is reversed (see also Sec. II A). This, in turn, affects the capacity of the system to retain information of the starting condition due to the importance of the sweeping rate in enhancing the likelihood of escape, especially in fluctuation distributions with larger jumps, which explains why R decreases significantly for larger sweeping amplitudes [see Fig. 3(d)].

For lower starting positions [L or I in Fig. 3(a)], the reverse scenario is observed [Fig. 3(d)]. As the forward sweeping maximum λ amplitude is increased the more efficient the asymmetry is; towards larger values all starting positions attain roughly a selectivity of 80% and 60% for Gaussian and Lévy noises, respectively. A similar reasoning as that presented above is valid here. Yet the tendency observed is that larger amplitudes lead to an improvement of the effectiveness of g as a state selector in the face of fluctuations.

The effect of the distribution of fluctuations is once again verified, especially for starting positions L and I [see Fig. 3(a)]: the Lévy distribution leads to lower selectivities for larger sweeping amplitudes, i.e., when proximity of sample paths to the unstable state is more probable. On the other hand, the larger asymmetry for positive jumps in ξ [see Eq. (4)] when a Lévy noise term is used works to increase the relative R if lower sweeping amplitudes are imposed, i.e., when distances to the unstable branch are such that the Gaussian noise is not as successful in eliciting jumps into the basing of attraction of the selected branch. Despite the fact that the Lévy distribution has a long tail towards positive jumps, which effectively secured an overwhelming bias towards the positive branch for a very particular case when one-way only dynamic bifurcations were tested (Sec. II A 1), the results plotted in Fig. 3(d) were derived with $\sigma = 0.1$ and final $\lambda = -2$. At this amplitude the imbalance towards the upper branch is still relatively minor [see Fig. 2(b) and Eqs. (6) and (5)], and its success in increasing selectivity is secured only in conjunction with the other ingredient tested in this section. This synergy is, in many ways, similar to that observed in Fig. 3(c), where lower sweeping rates exert a similar action to that of larger sweeping amplitudes. We must also add that the order of the respective selectivity curves is consistent with the distance of the initial conditions to the steady state favored by g.

III. DISCUSSION AND FURTHER WORK

Several important contributions stemming from nonequilibrium physics have been applied to the problem of information processing in biocircuits [27,45,46]. The equally rich field of open systems [13,15,17] and dynamic bifurcations [14,35], which deals with equivalent problems, has been less utilized in the interpretation of biological intracellular phenomena. The mechanism of Speed-dependent Cellular Decision Making, initially proposed in Ref. [11] and further advanced in Ref. [18] contributes to the expansion of this field in biology. Here we developed the framework further by testing the ability of dynamically bifurcating systems to retain memory of initial conditions in the face of forward-reverse sweeping through critical regions and heavy-tailed noise distributions. This systematic investigation is clearly in line with the effects of complex signals that dictate encoded evolutionary responses to environmental pressures. Moreover, asymmetric heavy-tailed Lévy distributions have recently been proposed as viable alternatives that naturally incorporate large deviations even at small noise amplitudes. In order to analyze clearly all of the elements underlying rate-dependent phenomena in fluctuating systems, we resorted once more to the paradigmatic bistable potential problem undergoing a supercritical Pitchfork bifurcation. This simple system was proven to exhibit similar characteristics to representative intracellular circuits and constituted a simple approach allowing for thorough computational tests.

Overall, sweeping through the critical region at different rates has different effects on correct branch identification when we start at different initial conditions in forward-backward dynamic bifurcations. Whereas a slow passage through the critical region may help to process the information carried by an external asymmetry and, additionally, a gradual increase in sweeping rates degrades this sensitivity, this is only strictly true in forward bifurcations from a monostability to a bistability region. In forward-backward sweeps, if the system starts at the branch favored by the external signal, monotonicity of state selectivity with sweeping rate is not observed. A region in the vicinity of sweeping rates close to 1 hinders both the maintenance of memory of initial conditions and the effect of external asymmetries. For initial conditions not in the attractor basins of the state favored by the external signal, the gradual tendency with sweeping rates is similar to that observed in previous studies.

Moreover, it is the combination of sweeping speed and noise distribution that allows for a robust memory of starting conditions. Heavy-tailed distributions can destroy all information encoded in an external signal if the sweeping speed is not adapted to the starting point and the amplitude of maximal deviation in a forward-reverse dynamic bifurcation. Additional tests on other bifurcations that can explain decision making in biology [10,21,47] should also reveal specific balances between bifurcation type, type of external signal, and unexpected rate-dependent effects contributing to correct information processing in the face of large fluctuations.

Regarding the rate-dependent forward-reverse dynamic bifurcation as a mechanism for decision making, we observed that, if sweeping speeds and amplitudes are sufficiently low and high, respectively, this is fundamentally a more efficient strategy for processing signals than attractor to attractor transitions over potential barriers, if the system is initially at a "suboptimal" position. The latter decision-making mechanism has been accepted in the literature as a strategy used by biocircuitry under uncertainty. The field of dynamic bifurcations has been less explored as a tool. Yet, as was proven in previous work and in the present paper, it is a viable alternative that should be explored in real cellular networks.

ACKNOWLEDGMENT

A.Z. acknowledges support from Russia (RU) under Grant No. 074-02-2018-330.

[1] V. Shahrezaei, J. F. Ollivier, and P. S. Swain, Mol. Syst. Biol. **4**, 196 (2008).
[2] C. G. Bowsher and P. S. Swain, Proc. Natl. Acad. Sci. USA **109**, E1320 (2012).
[3] C. G. Bowsher, M. Voliotis, and P. S. Swain, PLoS Comput. Biol. **9**, 1 (2013).
[4] J. Dattani and M. Barahona, J. R. Soc. Interface **14**, 20160833 (2017).
[5] V. Mustonen and M. Lässig, Phys. Rev. Lett. **100**, 108101 (2008).
[6] V. Mustonen and M. Lässig, Trends Genet. **25**, 111 (2009).
[7] R. A. Gatenby, A. S. Silva, R. J. Gillies, and B. R. Frieden, Cancer Res. **69**, 4894 (2009).
[8] A. Fischer, I. Vázquez-García, and V. Mustonen, Proc. Natl. Acad. Sci. USA **112**, 1007 (2015).
[9] D. Palau-Ortin, P. Formosa-Jordan, J. M. Sancho, and M. Ibañes, Biophys. J. **108**, 1555 (2015).
[10] S. Huang, Y.-P. Guo, G. May, and T. Enver, Dev. Biol. **305**, 695 (2007).
[11] N. R. Nené, J. Garca-Ojalvo, and A. Zaikin, PLoS ONE **7**, e32779 (2012).
[12] N. R. Nené and A. Zaikin, PLoS ONE **7**, e40085 (2012).
[13] M. C. Cross and P. C. Hohenberg, Rev. Mod. Phys. **65**, 851 (1993).
[14] N. Berglund and B. Gentz, *Noise-Induced Phenomena in Slow-Fast Dynamical Systems: A Sample-Paths Approach*, Probability and Its Applications (Springer, London, 2006).
[15] C. Hobbs, P. Ashwin, S. Wieczorek, R. Vitolo, and P. Cox, Phil. Trans. R. Soc. A **371**, 20130098 (2013).
[16] P. Ashcroft and T. Galla, Phys. Rev. E **88**, 062104 (2013).
[17] C. Perryman and S. Wieczorek, Proc. R. Soc. A **470**, 20140226 (2014).
[18] N. R. Nené and A. Zaikin, Phys. Rev. E **87**, 012715 (2013).
[19] A. Alagha and A. Zaikin, Front Immunol. **4**, 426 (2013).
[20] B. Pfeuty and K. Kaneko, Phys. Biol. **6**, 046013 (2009).
[21] T. Enver, M. Pera, C. Peterson, and P. W. Andrews, Cell Stem Cell **4**, 387 (2009).
[22] C. Schröter, P. Rué, J. P. Mackenzie, and A. Martinez Arias, Development **142**, 4205 (2015).
[23] Y. Xu, Y. Li, H. Zhang, X. Li, and J. Kurths, Sci. Rep. **6**, 31505 EP (2016).
[24] Q. Liu and Y. Jia, Phys. Rev. E **70**, 041907 (2004).
[25] J. Jaruszewicz and T. Lipniacki, Phys. Biol. **10**, 035007 (2013).
[26] E. Kussell and M. Vucelja, Rep. Prog. Phys. **77**, 102602 (2014).
[27] T. J. Kobayashi, Phys. Rev. Lett. **106**, 228101 (2011).
[28] F. Moss, D. Kondepudi, and P. V. McClintock, Phys. Lett. A **112**, 293 (1985).
[29] D. K. Kondepudi and G. W. Nelson, Phys. Rev. Lett. **50**, 1023 (1983).
[30] C. Nicolis and G. Nicolis, Phys. Rev. E **62**, 197 (2000).
[31] G. Nicolis and C. Nicolis, Physica A **351**, 22 (2005).
[32] C. Nicolis and G. Nicolis, New J. Phys. **7**, 8 (2005).
[33] R. Guantes and J. F. Poyatos, PLoS Comput. Biol. **4**, e1000235 (2008).
[34] V. Chickarmane, T. Enver, and C. Peterson, PLoS Comput. Biol. **5**, e1000268 (2009).
[35] T. Erneux, E. Reiss, L. Holden, and M. Georgiou, in *Dynamic Bifurcations* (Springer-Verlag, Berlin, Heidelberg, 1991), pp. 14–28.
[36] D. Kondepudi, F. Moss, and P. V. McClintock, Phys. D **21**, 296 (1986).
[37] S. Grossmann and A. Mikhailov, Zs. Phys. B Condensed Matter **78**, 1 (1990).
[38] C. W. Gardiner, *Handbook of Stochastic Methods for Physics, Chemistry and the Natural Sciences* (Springer-Verlag, Berlin, Heidelberg, 1994).
[39] S. L. Werner, D. Barken, and A. Hoffmann, Science **309**, 1857 (2005).
[40] M. Behar and A. Hoffmann, Curr. Opin. Genet. Dev. **20**, 684 (2010).
[41] L. O. Murphy, S. Smith, R.-H. Chen, D. C. Fingar, and J. Blenis, Nat. Cell Biol. **4**, 556 (2002).
[42] C. Nicolis and G. Nicolis, Phys. Rev. E **67**, 046211 (2003).
[43] C. G. Bowsher and P. S. Swain, Curr. Opin. Biotechnol. **28**, 149 (2014).
[44] J. W. Young, J. C. Locke, and M. B. Elowitz, Proc. Natl. Acad. Sci. USA **110**, 4140 (2013).
[45] J. Berg, Phys. Rev. Lett. **100**, 188101 (2008).
[46] H. Ge and H. Qian, Phys. Rev. Lett. **103**, 148103 (2009).
[47] J. Wang, K. Zhang, L. Xu, and E. Wang, Proc. Natl. Acad. Sci. USA **108**, 8257 (2011).